

Focal Zones of Earthquakes Modeled in Terms of the Lattice Regularization

V. I. Ulomov

Schmidt Joint Institute of Physics of the Earth, Russian Academy of Sciences,
Bol'shaya Gruzinskaya ul. 10, Moscow, 123810 Russia

Received October 30, 1996; in final form, November 24, 1997

Abstract—A fractal lattice model of the space–time and energy development of seismogeodynamic processes is used to discuss the identification and numerical parametrization of earthquake source zones (ESZ) for solving seismic risk zoning problems. Four scale levels of observed and predicted seismicity effects are considered: a seismically active region and its three basic structural elements including lineaments, domains, and potential earthquake sources. The joint analysis of seismic regime at these scale levels substantiate the concept developed in this paper. A new technique (Adequate Earthquake Source Technology-97) for the creation of probabilistic–determinate ESZ models and for their application to the seismic zoning is proposed and illustrated with an example of the Crimea–Caucasus–Kopet Dagh region, which is the test area of the International Program on the Global Seismic Risk Assessment.

INTRODUCTION

Until recently, the most complicated problem of seismic zoning and long-term prediction of large earthquakes has been the identification of earthquake source zones (ESZ) and estimation of their seismicity parameters. Investigations that were conducted in our country and resulted in a change of the seismostatistical paradigm in the 1950–1960s formed a basis for the genetic two-stage seismic zoning and statistical assessment of seismic risk [1–4]. According to this concept, the seismogenic zones are to be identified at the first, seismotectonic stage [1], and the related seismic effects on the surface are estimated at the second, engineering stage. The two-stage pattern and statistical approach to the mapping of the seismic risk have been widely used in seismology throughout the world, especially after the well-known works by Cornell and his followers [5–10]. However, in spite of a high efficiency of this method, the second stage of seismic zoning studies, namely the calculation of probability of the seismic surface effect, has been mostly developed. The first stage (the identification and seismic parametrization of source zones), which addresses deep seismogeodynamic processes and involves seismologists, geologists, and geophysicists, is less developed and, to a great extent, biased. A more or less formalized method of the identification of quasi-homogeneous zones generating seismic waves was described by Keilis–Borok *et al.* [11]. Nonetheless, the approaches proposed at that time, as well as similar methods that have become familiar in the past decades [12], can be considered only as a first approximation to the seismotectonic zoning, since they do not reflect the regional seismicity features, energy of large blocks, and dynamics of seismogenic linear structures crossing the quasi-homogeneous zones.

Our long-term investigations are based on the two-stage principle implying the creation of two mutually related prediction models: a model of source zones (MSZ) and a model of seismic effect (MSE) (Fig. 1). However, the results presented below concern mainly the MSZ model which is based on the lattice regularization and includes basically new quantitative parameters and their statistical estimates [13–16]. The study area includes entire North Eurasia, but the most detailed studies were carried out for the Crimea–Caucasus–Kopet Dagh region, because it is an international test area for improving the methods of seismic risk assessment [12, 17].

LATTICE MODEL OF SEISMOGENESIS

In most countries, the seismic risk is defined as the probability that the maximum intensity of ground motions caused by all potential seismic sources in a region under study would not be exceeded during a given time interval. In this case, the sources of seismic shocks are simulated by a set of points, lines, and other simple geometric figures [5]. However, as mentioned above, the models thus constructed are suitable for engineering calculations, but they do not adequately reflect the seismic process.

The fractal lattice model (FLM), describing the energy evolution of seismogeodynamic processes in space and time, which we proposed in the mid-1980s, is fully suited for modeling the ESZ. This model is geometrically and physically reasonable and correctly parametrizes the seismic process. A basis for the construction and application of the model is the principle of the hierarchical ordering of geological structures,

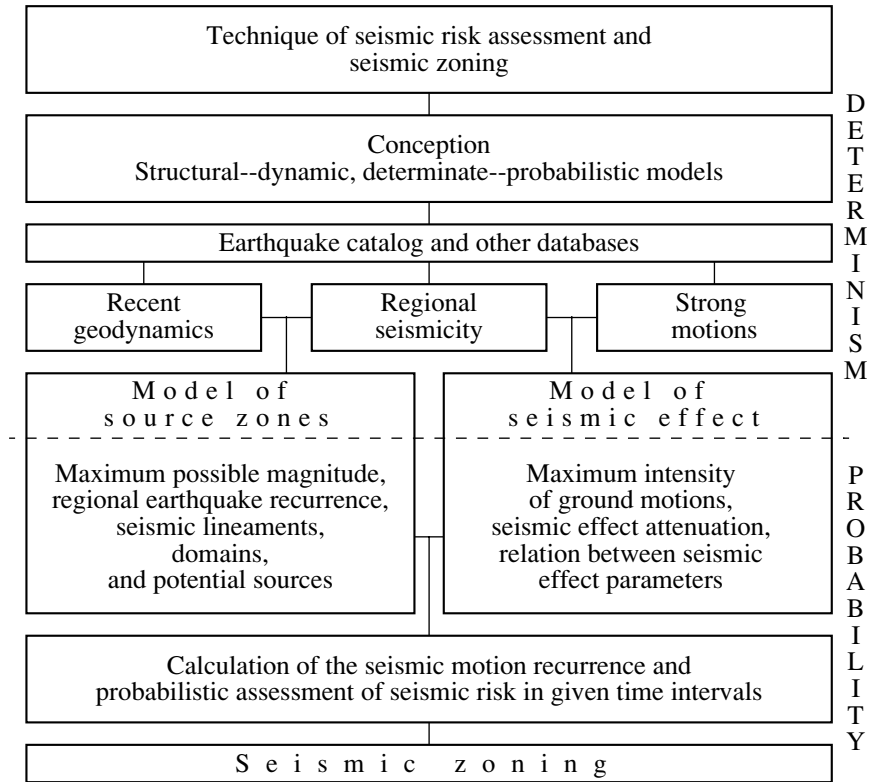


Fig. 1. Block diagram of the seismic zoning technique. Three (geodynamic, seismicity, and macroseisms) blocks of data bank, taken in pairs, form the source zone model and seismic effect model, which are used as a basis for estimating the seismic risk and for compiling the seismic zoning and risk maps. Like the seismic risk assessment, both zones are largely probabilistic.

geodynamic and seismic processes, and earthquake sources [13–16].

Other methods of the seismic source modeling are based on the continuum mechanics results [e.g. 3, 18–20], laboratory and field studies of rock failure, and other approaches described in [21]. However, we believe that FLM gives new possibilities for the better understanding of seismogenesis and for the effective use of tectonic, geodynamic, and seismic evidence for studying the space–time and energy distribution of seismicity. The introduction of the lattice regularization in seismic geodynamics enables the efficient application of up-to-date methods of synergy, fractal analysis, and percolation theory [13] to seismic studies.

Ordering of Seismically Active Structures

The seismic sources are not distributed chaotically. They arise in the most compliant interblock contact zones and most often occur, in a regular manner, in fixed areas that are least favorable for creep displacements and thereby seismically most hazardous. Commonly, these seismogenic structures are intersections of faults or displacement zones, their sharp bends, or other features (asperities and barriers) that prevent slow tectonic movement on faults. The dimension of such areas is determined by the sizes of interacting blocks

bounded by active faults or displacement zones. These sizes control the upper limit of the earthquake magnitude, and the number of blocks is responsible for the rank and intensity of the tectonic movements (average number of seismic events per unit time). The fault ranks J_i and the distances between their disjunctive nodes δ_j , as well as block sizes, are determined by the thickness and strength of the related layers faulted in the past geological epochs. The thicker the layer divided by faults into blocks, the larger and longer the faults and the greater the distances between them. This results in an increase in block sizes and, consequently, in the magnitude of the related earthquakes. Conversely, the number of faults, blocks and earthquake sources increases as the layer thickness decreases.

The lattice of the intracontinental faults is predominantly of the rectangular, or more often square shape determined by the tangential compression. Ulomov [13–16] showed that the distances δ_j between nodes and, consequently, the block sizes have a marked tendency to correlate with rank, the block sizes approximately doubling as their rank increases by unity. This effect is caused by the regular doubling of the depth of main interfaces in the crust and upper mantle (the granitic layer top, Conrad discontinuity, and bottoms of the crust, lithosphere, and asthenosphere occur, respectively, at depths of about 10, 20–25, 40–50, 80–100,

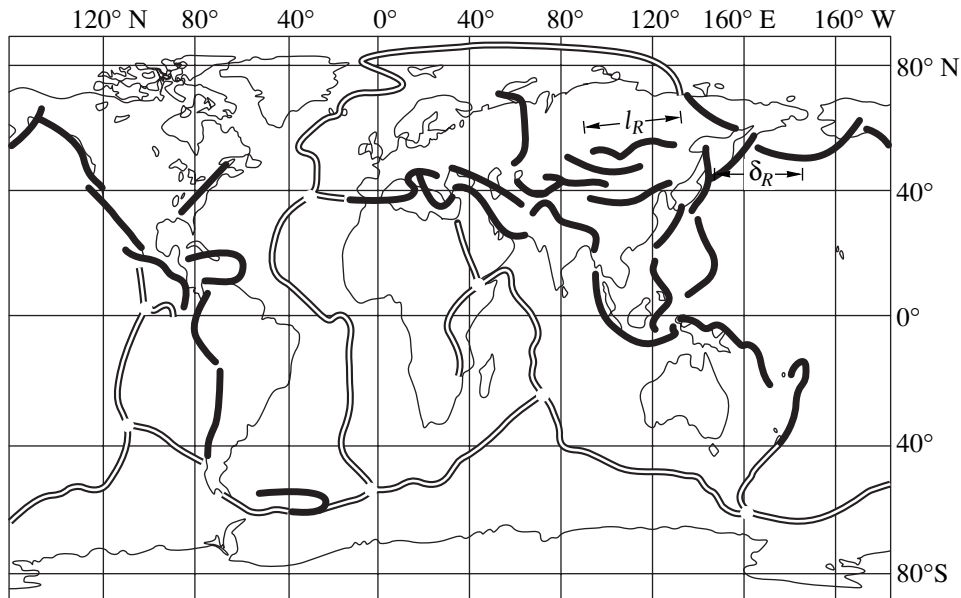


Fig. 2. Global ordering of the seismogenic regional structures. Bold lines are the axes of convergent subduction zones and their relicts on the continents. Double lines are the axes of divergent rift zones.

and about 200 km; the deeper boundaries occur at depths of about 400, 700 km, and so on). A regular hierarchical structure is also characteristic of seismogeodynamic activation disturbances of the solitary wave type (the so-called *G* waves, or geons), propagating along faults and activating earthquake sources through stress release at disjunctive nodes [22].

In order to determine the size of the areas δ_M responsible for the energy potential (magnitude M_{\max}) of earthquakes and to estimate the seismic geodynamic potential of the relevant blocks of size δ_j , we studied the spatial distribution of intracontinental earthquake sources in a wide range of magnitudes, from $M = 6.0 \pm 0.2$ to $M = 8.0 \pm 0.2$ (hereafter, unless otherwise noted, M means the magnitude M_{LH} determined from surface waves). For this purpose, we constructed the statistical function of the distribution of distances δ_M between the epicenters of the closest earthquake source pairs over fixed intervals $\Delta M = M \pm 0.2$, with a magnitude step of 0.5. The origin time of earthquakes was not taken into account, since, as mentioned above, we assumed that seismic sources are repeatedly activated at the same disjunctive nodes (fault walls rather rapidly stick together), and we were interested only in their location. It was found that earthquake sources quantized in magnitude M or energy E (in joules) are regularly distributed in both time (the Gutenberg–Richter law, the τ_M function) and space (δ_M function), clearly demonstrating the space and time symmetry inherent in the nature.

Statistically averaged distances δ_M or δ_K (in km) between the epicenters of the nearest earthquake sources with magnitudes fixed within an interval of

$\Delta M = \pm 0.2$, or with energies from an interval of $\Delta K = \pm 0.5$, are described by relations with small dispersion. (The standard deviations of sources from their statistically mean coordinates vary within an interval equal to the twofold source size L_M . This corresponds to the probability $P \approx 0.7$ in the distribution function of potential sources on segments of length δ_M , oriented along seismogenic structures [13]). These relations are

$$\log \delta_M = 0.6M - 1.94; \quad \log \delta_K = 0.333K - 3.272, \quad (1)$$

where $K = \log E = 1.8M + 4.0$.

The relation between the earthquake source sizes (length) L_M (in km) and their magnitudes M , which is obtained both analytically and statistically, is described as

$$\log L_M = 0.6M - 2.5; \quad \log L_K = 0.333K - 3.832. \quad (2)$$

The factor 0.6 at M implies that the source size L_M and distances between epicenters δ_M change approximately by a factor of two with a 0.5 increase in magnitude. According to (1) and (2), the value of $\delta/L \approx 3.63$ is magnitude-invariant and reflects the hierarchical self-similarity of block sizes and earthquake sources in the whole magnitude interval considered (from $M = 6.0 \pm 0.2$ to $M = 8.0 \pm 0.2$). Our study showed that physically more reasonable relations can be used for the seismic modeling with the help of the lattice principle:

$$L = 2^{\log E / \sqrt{3.5}}; \quad \delta = 2^{\log E / \sqrt{3.5}}. \quad (3)$$

Being equivalent to (1) and (2), these relations are more suitable for the representation in the SI units (L and δ in meters and energy E radiated by the source, in joules).

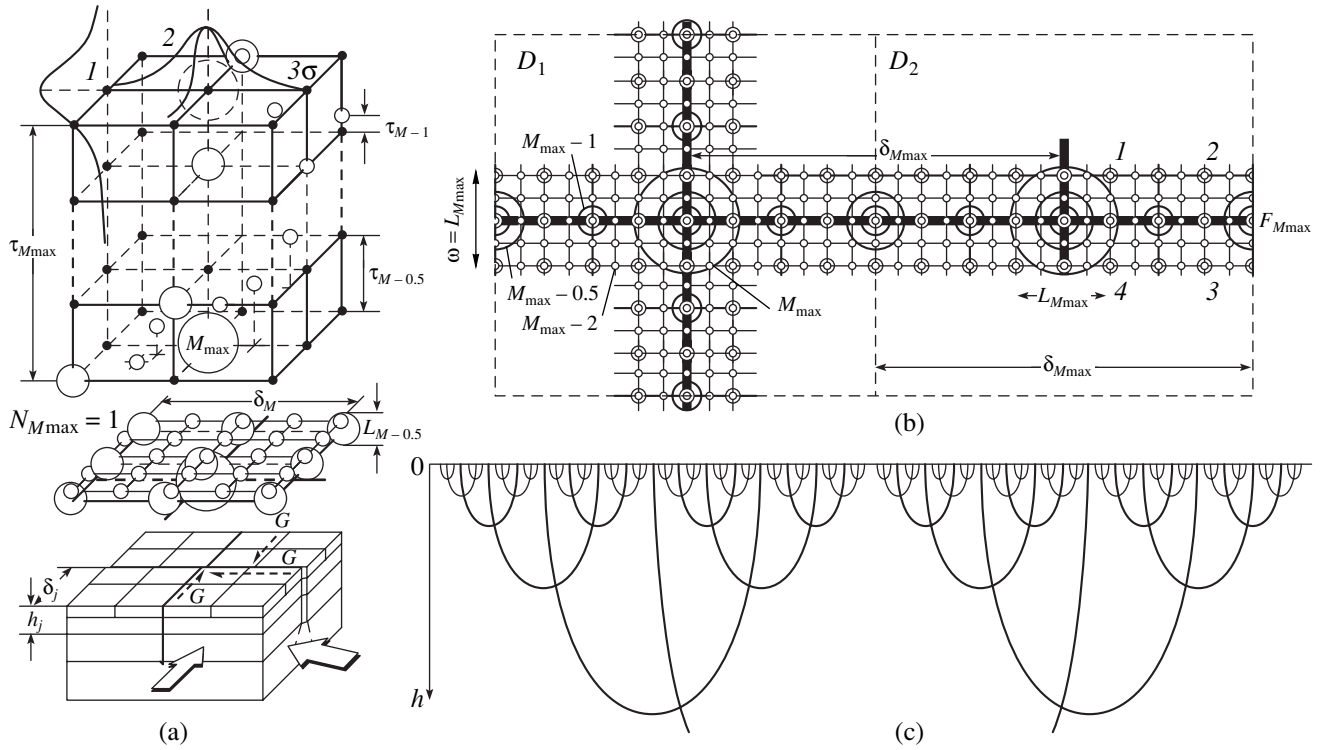


Fig. 3. (a) Unit cell of the ordered fractal lattice model (FLM) of seismogenesis and (b) an idealized model of the earthquake source origination. The circles of diameter L_M show the sources with M_{\max} , $M_{\max}-0.5$, and $M_{\max}-1$ (Fig. 3a) and the M_{\max} to $M_{\max}-2$ sources (Fig. 3b). Figure 3c illustrates a more realistic example of the transverse vertical section of an ordered system of arcuate faults with a fractal dimension similar to that of the blocks ($U \approx 0.667$). The probabilistic-determinate character of the FLM is reflected in the curves of the random distribution of events in (1) time and (2) space, shown at the top of Fig. 3a. For other explanations, see the text.

Thus, δ characterizes the average cross-sectional dimension of a block that can generate earthquakes of the maximum magnitude M_{\max} in each of its (on average, four) dislocation nodes.

We showed that statistically mean distances δ_R between the geometric centers of main seismically active regions of the world and their lengths l_R , corresponding to the maximum possible amplitude of $M_{\max} \approx 9$, are also described by relations (1) and (2) (Fig. 2) [13–16]. We also revealed other regularities which adequately characterize regional seismicity and development of seismogeodynamic processes.

Fractal Lattice Model of Seismogenesis

The ordering relations between blocks, seismic sources, and development of seismogeodynamic processes underlie a generalized fractal energy-space-time lattice model (FLM) of the seismogenic process, which we proposed more than ten years ago [13]. Contrary to the traditional continuous models, which integrate the discrete seismicity [3], this model most adequately reflects the diversity, regularity, and coherence of the discrete structure of a geophysical medium and “quantum” dynamics of seismic processes (Fig. 3).

The introduction of the lattice regularization, fractals, and synergy effects in the seismic geodynamics is not only a convenient mathematical description, but also a useful tool for better understanding of the earthquake nature and for solving fundamental and applied seismic problems. This idealized model, in spite of (rather, due to) its formalism can be easily analyzed numerically and provides a deeper insight into the physical essence of seismic phenomena. The FLM incorporates the concepts of geometric and energy similarity in the hierarchical layered block structure of the crust and upper mantle, self-similarity of seismic phenomena, and confinement of various earthquake sources to disjunctive tectonic nodes (intersections and bends of faults, stronger inclusions in interblock contact zones, and so on).

Figure 3a (the middle part) shows an elementary cell (EC) of the FLM, which may be considered as a domain under the dynamic effect of a maximum magnitude (M_{\max}) earthquake source located at the center of the domain. The FLM is a hierarchically ordered three-dimensional tetragonal lattice, dividing an energy accumulating into blocks and imitating fault lineaments or other linear tectonic structures. The earthquake sources, shown as L_M -diameter spheres and quantized at a 0.5 step in magnitude, are located at the δ_M -spaced

FLM nodes¹. This source lattice is a part of the hierarchically constructed block shown at the bottom of Fig. 3a. Earthquake focuses (FLM nodes) and axes of the corresponding faults (FLM connections) are arbitrarily located at depths h_M equal to $L_M/2$. The FLM structure as a whole is based on relations (1) and (2), and the scaling factor is 2 at a magnitude step of 0.5.

The earthquake occurrence in time is controlled by the time hierarchy step τ_M . This step is dependent on the recurrence of seismic events with $M < M_{\max}$ within the EC of the maximum earthquake during its cycle $\tau_{M_{\max}}$ (Fig. 3a, on the top). Both the spatial (δ_M) and time (τ_M) FLM periods decrease as M diminishes. Small and large steps of the lattice correspond to weak and strong earthquakes. A negligibly small step means the white noise, and the maximum step corresponds to the strongest earthquake with $M = M_{\max}$. The FLM ECs (similar to the natural conditions) can be complete or incomplete, depending on their structure and source distribution at their nodes (for example, truncated ECs of narrow ESZs, sources that have or have not released seismic energy in a fixed time interval, and so on).

Applying affine transformations, which leave the model physically unaffected, we can transform spheres into three-axial ellipsoids, introduce anisotropy, and so on, making the model more realistic.

The curves of statistical distribution of events in time (1) and space (2), shown in Fig. 3a, provide a probabilistic basis for the FLM model which at first glance looks as highly deterministic.

The reliability of the model can be enhanced by incorporating experimentally observed space-time and magnitude distributions of earthquake sources, as is schematically shown in the upper part of Fig. 3a for a potential source with M_{\max} . Such a model includes standard deviations σ_δ , σ_τ , and σ_M from their average values obtained in terms of the simpler FLM. Thus, we found that, for earthquakes in Central Asia, the values of $3\sigma_\delta$ are commonly not greater than $\delta_M/2$, which is half the averaged distance between the earthquake epicenters with a given M (see Fig. 3a). In other words, both the model and real conditions show that the majority of sources with M_{\max} are located within their domain and almost 70% of the sources deviate from their "ideal" position only by a value equal to the twofold size of the seismic source L_M . This is also valid for the seismic regime controlled by the value τ_M .

¹ The 0.5-magnitude sampling step was not chosen arbitrarily. The ordering of the hierarchical distribution of lithospheric blocks, which we have previously revealed (grouping of rank-variable blocks and doubling of their linear dimensions), indicates the earthquake energy to be naturally discrete, with a M_s step of about 0.6. Obviously, the energy of the blocks generating seismic waves should be accepted as a basis for the magnitude classification of earthquakes in place of the conventional magnitude scale presently used in seismology (a possible exception is the moment magnitude M_w which is physically more adequate).

Every EC with a size of $\delta_{M_{\max}}^2$ (D_1 and D_2 in Fig. 3b) is the preparation zone for an earthquake with the magnitude M_{\max} and is responsible (and sufficiently large) for the total number N_M of the sources of earthquakes with $M < M_{\max}$ that occur during one cycle $\tau_{M_{\max}}$ within this EC. The recurrence plot of the seismic events with $M < M_{\max}$ within a single EC (individual earthquake recurrence plot) can be obtained from the known expression

$$\log N_M = \log N_0 - b(M - M_0),$$

replacing M_0 by M_{\max} and accepting $N_0 = N_{M_{\max}} = 1$.

Hence,

$$\log N_M = b(M_{\max} - M), \quad (4)$$

where b is the slope of the earthquake recurrence plot, which reflects the fractal dimension of the set of seismic events. In the SI units and for the energy scale of earthquake intensities, this value is

$$\gamma = -\log N_K / \Delta K \approx 0.667.$$

Now, we show that the layered-block structure of a geophysical medium has the fractal dimension U_c similar to the dimension of the source seismicity structure γ in terms of its energy classification (the magnitude classification is unacceptable in this case; the only exception is the seismic moment M_0 reflecting the energy spent to produce seismic movement). As seen from Fig. 3a (at its bottom), the number N_j of ordered blocks depends on the unit of measurement of the volume $V_j = \delta_j^2 h_j$, where δ_j^2 and h_j are, respectively, lateral and vertical sizes of a block in the generation considered. As noted above, at each step of generation, one large block (j) is replaced by four above lying blocks of the lesser, ($j - 1$)th rank; i.e., $N_j/N_{(j-1)} = 4$. The volume of each new block V_j is 1/8 of the volume of the preceding one, since only the upper half of the block is divided into four parts; the lower half remains intact and adjacent to the underlying layer, which was not affected by the faulting process of this rank. Hence,

$$U_c = -\log 4 / \log(1/8) = 0.(6) \approx 0.667.$$

All this indicates the structural-dynamic coherence of the hierarchical geophysical medium and the processes that occur within it.

To clarify the physical nature of fractals, we note that if the division into blocks were performed in a different manner, namely, if every block as a whole (rather than its upper half) were divided at each step into eight parts, the dimension of the generation would be Euclidean, since $\log 8 / \log(1/8) = 1$.

The fractal dimension actually reflects the properties of scale invariance, implying that self-similarity effects cause the whole to be, in a way, similar to its parts, and, vice versa, the parts are similar to the whole. The tectonic activity caused by the lithospheric plate

movements, faults and blocks of the crust and lithosphere, and therefore earthquake sources continuously produce regular self-similar fractal structures, since this is the most economical and simple way of rearrangement of a deformed and fractured geophysical medium; undisturbed portions of the medium between large objects continue to divide similar to the Kantor set. Their number continuously increases. The faults, blocks, and earthquake sources become progressively smaller, gradually filling the whole space (Fig. 3c). The lines of faults of various ranks cover the ground surface by a dense mesh and acquire a fractional, fractal dimension, which is intermediate between a line and plane. Deep fault planes divide the crust and lithosphere into blocks whose fractal dimension tends to the three-dimensional topological dimension. There are no dominating scale ranges, and this is the main property of the self-similarity.

Another important property inherent in the FLM (as well as of the natural medium), controlling its dynamic behavior and forming earthquake sources at its nodes, is the soliton-like stress and strain waves (the so-called geons [22]), which propagate along the hierarchical FLM boundaries and determine the directivity of development of seismic geodynamic processes in nature (the open arrows at the bottom of Fig. 3a indicate the direction of the G -wave movement along the faults).

Obviously, the real location and structure of faults and blocks, as well as the energy–space–time distribution of earthquake sources, are not so perfect and determinate as those in our lattice model. The real medium is also imperfect due to its nonlinearity, inhomogeneity, and entropy processes, which develop concurrently with self-organizing processes. Thus, blocks do not have a rectangular or square shape, and faults are not vertical. These structures are more complicated (and have, for example, an arc-like shape, see Fig. 3c), but this does not change the essence of the method. In principle, we can introduce the lattice regularization and construct a satisfactory fractal model for any apparently chaotic system in which some ordering and scale similarity are recognizable.

Lineament-Domain-Source Model of Source Zones

Thus, the FLM description of earthquake source zones includes three basic structural elements: (1) lineaments modeling active faults or displacement structures of various energy ranks, along which earthquake sources are distributed; (2) domains involving quasi-homogeneous blocks of the geophysical medium, subjected to the dynamic action of basic linear structures and large earthquake sources; (3) sources of potential earthquakes of various magnitudes, which are adjacent to related disjunctive nodes.

The model of extended source zones of M_{\max} earthquakes is constructed through successive translations

of ECs along the corresponding axes $F_{M_{\max}}$ imitating the seismoactive linear structures (Fig. 3b). As noted above, the domains D_1 and D_2 shown in Fig. 3b are the areas of preparation of the corresponding earthquake sources with M_{\max} within the interval δ_M . These areas are also responsible for the set of N_M sources of earthquakes with $M < M_{\max}$, occurring during one cycle $\tau_{M_{\max}}$ within this EC. The ESZ width ω defines the width of the area, dynamically affected by major central faults $F_{M_{\max}}$. The meanings of other source zone parameters is clear from Fig. 3b.

Using the FLM, it is easy to understand changes in the slope b and curvature of the recurrence plots observed in reality, depending on the layering and fragmentation degree of the geophysical medium, length-to-width ratio of seismically active zones, and other parameters. For example, the most frequently observed value $b = 0.9$ characterizes seismically active structures whose width w (ω in Fig. 3b) is comparable with the source length $L_{M_{\max}}$ of the maximum possible earthquake within these structures (in the case of an “incomplete” EC, $\omega \approx \delta/4$). In the case of a “complete” EC, $\omega = \delta$ (for example, the elementary $M_{\max}-1$ cell marked by points 1 to 4 in Fig. 3b), the b value of the individual recurrence plot of earthquakes with $M < M_{\max} - 1$ attains the highest value $b = 1.2$.

Other specific features of the seismic regime, which are not obvious in terms of the standard traditional approaches, are also revealed. For example, the FLM suggests that, at every tectonic node of the hierarchical structure, a source of earthquakes with $M < M_{\max}$ can arise within the area of the size $\delta_{M_{\max}}^2$, on average, once per cycle $\tau_{M_{\max}}$ corresponding to the recurrence of the maximum earthquake with M_{\max} that may occur in this area.

SEISMOLOGICAL PARAMETRIZATION OF SOURCE ZONES

Regional Structure of ESZs

The ordered regional pattern of global seismicity yields evidence of a close relationship between the seismically active intracontinental regions and relicts of the subduction that occurred here in the past geological epochs (Fig. 2) [15, 16]. These regions of a comparatively strong lithosphere, close in length to the present island arcs (3000 ± 500 km), are most intensely affected by deformation processes and, consequently, exhibit high seismic activity. Thus, each of these regions can be accepted as an “initial,” seismically active structure determining the specific seismicity features in the region considered (Fig. 4, Table 1).

The intraregional earthquakes do not arise in a homogeneous medium. They are initiated in a discrete layered-block medium whose hierarchical structure is predetermined by previous geological epochs and is eventually governed by Neogene–Quaternary and

Table 1. Seismic zoning of North Eurasia (see Fig. 4) [33, 35]

Segments and regions	Geographical coordinates of the main segments (1–4) and regions (latitude N and longitude E everywhere unless otherwise noted)			
0—North Eurasia (the general outline)	90–20	44–20	44–22	40–22
	40–30	34–30	34–80	40–80
	40–164	50–164	50–174	60–174
	60–168W	90–168W		
1—East European segment (general outline)	90–20	44–20	44–22	40–22
	40–30	34–30	34–62	74–62
	74–70	90–70		
Regions:				
1.1—Iran–Caucasus–Anatolia	48–30	34–30	34–62	48–62
1.1.1—Crimea–Caucasus–Kopet Dagh subregion	46–31	42–31	42–37	35–37
	35–61	42–61	42–55	46–55
	50–20	44–20	44–22	40–22
1.2—Carpathians–Balkans	40–30	50–30		
	70–20	50–20	50–30	70–30
	70–30	48–30	48–56	70–56
1.3—Baltic region	70–56	48–56	48–62	70–62
1.4—Central and East Europe	90–20	70–20	70–62	74–62
1.5—Urals	74–70	90–70		
1.6—New Land				
2—Central Asian segment (general outline)	54–62	34–62	34–80	40–80
	40–102	44–102	44–90	46–90
	46–80	54–80		
Regions:				
2.1—Pamirs–Tien Shan	46–62	34–62	34–80	40–80
	40–102	44–102	44–90	46–90
	54–62	46–62	46–80	54–80
2.2—Central Kazakhstan	74–62	54–62	54–80	46–80
	46–90	44–90	44–102	40–102
	40–122	58–122	58–110	76–110
3—Central Siberian segment (general outline)	76–70	74–70		
Regions:				
3.1—Altai–Sayany–Baikal	58–80	46–80	46–90	44–90
	44–104	48–104	48–122	58–122
	74–62	54–62	54–80	58–80
3.2—West Siberia	58–110	76–110	76–70	74–70
	48–104	44–104	44–102	40–102
	40–122	48–122		
3.3—East Mongolia	90–70	76–70	76–110	58–110
	58–122	40–122	40–164	50–164
	50–174	60–174	60–168W	90–168W
Regions:				
4.1—Kuriles–Kamchatka	58–146	44–146	44–140	40–140
	40–164	50–164	50–172	60–172
	60–158	58–158		
4.2—Sakhalin–Japan	58–140	46–140	46–138	40–138
	40–140	44–140	44–146	58–146
	58–122	40–122	40–138	46–138
4.3—Amur–Primorski Krai	46–140	58–140		
	76–110	58–110	58–158	76–158
	90–70	76–70	76–168W	90–168W
4.4—Verkhoyansk	76–158	60–158	60–168W	76–168W
4.5—Northern Land				
4.6—Chukot Peninsula				

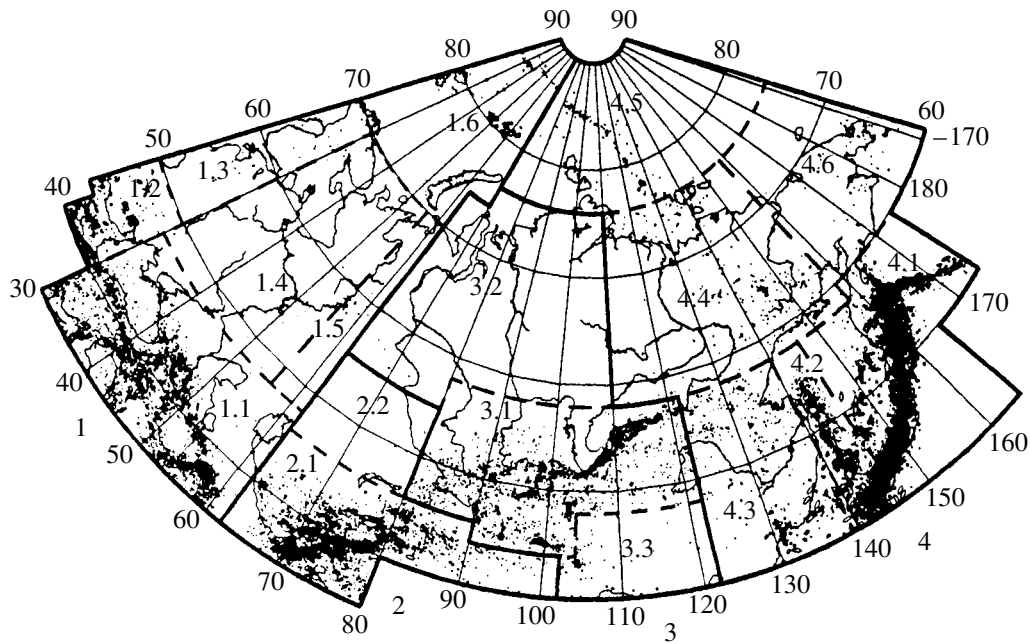


Fig. 4. Seismic zoning of North Eurasia. Segments: 1, East Europe; 2, Central Asia; 3, Central Siberia; 4, East Asia. Regions: 1.1, Iran–Caucasus–Anatolia; 1.2, Carpathians–Balkans; 1.3, Baltic region; 1.4, East Europe; 1.5, Urals; 1.6, New Land; 2.1, Pamirs–Tien Shan; 2.2, Central Kazakhstan; 3.1, Altai–Sayany–Baikal; 3.2, West Siberia; 3.3, East Mongolia; 4.1, Kuriles–Kamchatka; 4.2, Sakhalin–Japan; 4.3, Amur–Primorski Krai; 4.4, Verkhoyansk; 4.5, Northern Land; 4.6, Chukot Peninsula. The earthquake sources are from the Specialized earthquake catalog for the seismic zoning of North Eurasia (edited by N.V. Kondorskaya and V.I. UloMOV) for $M \geq 5.0$ from ancient times to 1995 and for $M \geq 3.5$ from 1960 to 1991 (the database of the Joint Institute of Physics of the Earth, Russian Academy of Sciences).

recent tectonic movements. The ESZs revealed in each seismically active region (R) and in the interregional space (the regions are not perfectly isolated from each other) depend on the geometry of long-lived seismically active faults and, as noted above, include seismogenic structures of three types: lineaments, domains, and potential sources of earthquakes (Fig. 5). All these structures are basic constituents of the lineament–domain–source (LDS) model considered below.

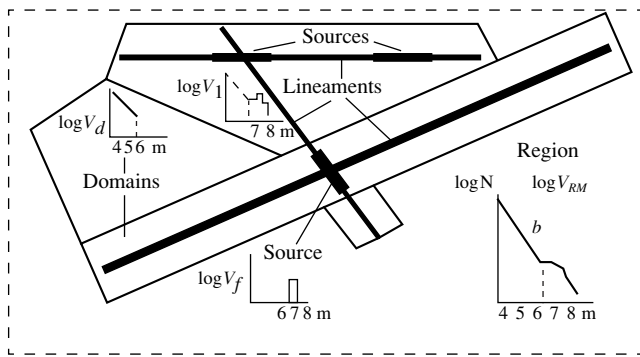


Fig. 5. Main structural elements of the LDS model of ESZs. The plots show the yearly average flux rate V of seismic events in the entire region R_i (V_{RM}) and its structural elements: lineaments (V_1), domains (V_d), and potential earthquake sources (V_f). One can see the magnitude intervals common to each of these structural types.

In order to identify the structures generating seismic waves and to estimate their seismic potential, it is important to use the mapping of the sources of earthquakes with various magnitudes in accordance with their size and orientation (Fig. 6) rather than the mapping of abstract “point” epicenters as is commonly done. The size and orientation of source are determined from the distribution of aftershocks, coseismic ruptures, maximum isoseismal lines, focal mechanisms, geodetic measurements, analysis of tectonic events, and so on. In accordance with the inferred relations and map legend proposed by UloMOV [23], sources of earthquakes with $M \geq 7$ ($M \geq 6.8$) are shown as ellipsoids. The large L and small W axes of the ellipsoids, as well as the conventional diameters L' of spheres for weaker sources, are calculated by the formulas conjugated at the level $M = 6.5$:

$$\begin{aligned} M \geq 6.5: \log L &= 0.6M - 2.5; \\ \log W &= 0.15M + 0.42; \\ \log(L/W) &= 0.45M - 2.92; \end{aligned} \quad (5)$$

$$M \leq 6.5: \log L' = 0.24M - 0.16.$$

Seismic lineaments, which serve as a basic frame of the LDS model, are a generalized surface reflection of the upper edges of three-dimensional, rather distinct, seismically active structures (Fig. 7). They outline blocks with relatively small differentiation of tectonic

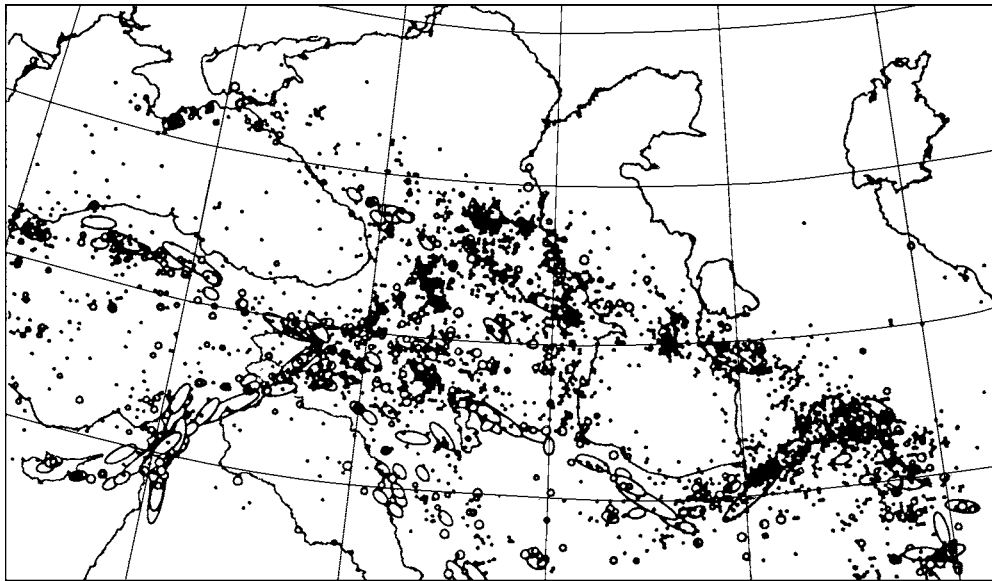


Fig. 6. Map of source seismicity in the Iran–Caucasus–Anatolian region and adjacent territory. Earthquake sources: $M \geq 8.0 \pm 0.2$ (large ellipses 200 km in length), $M = 7.5 \pm 0.2$ (moderate ellipses 100 km in length), and $M = 7.0 \pm 0.2$ (small ellipses 50 km in length); the circle diameters are proportional to the sources with M ranging from 6.5 ± 0.2 to 3.5 ± 0.2 , with a step of 0.5 [17].

movements and trace the junctions of blocks highly contrasting in tectonic activity. The lineaments are identified mainly with the help of the cluster or percolation analysis applied to the space–time distribution of earthquakes with pertinent magnitudes, which occur along the lineaments (Fig. 8). The lineaments can be also recognized from the geophysical fields (particularly, their gradients), satellite photographs, similar history of tectonic development in the Cenozoic (predominantly, Early Pleistocene and Holocene), Quaternary activity, similar values of neotectonic velocity gradients, and other specific features of neotectonic and present geodynamics. Dating of large paleoearthquakes is particularly important for studying the present space–time pattern of related faults and linear structures.

In practice, for the convenience of discretization and numerical analysis of the seismic effect (all computations are performed in the VLSI technology), extended lineaments are represented as broken lines, consisting of linear segments which may be considered as independent seismic sources of earthquakes of the same magnitude, distributed along these segments. The lineaments and their segments are characterized by the length l_i and width w_i dependent on their tectonic nature and localization uncertainties; the depths of the lower (H_{\min}) and upper (H_{\max}) edges of the fault plane; strike azimuth Az° ; dip angle α° ; and type of dominating movements (lateral and normal faults, thrusts, and so on). In the case of crustal earthquakes of various magnitudes, the value of H_{\min} commonly coincides with the top depth of the consolidated crust; the value of H_{\max} is related to the magnitude M_{\max} as follows: $H_{\max} = 10$ km for $M_{\max} \leq 4.5$; $H_{\max} = 15$ km for $5.0 \leq M_{\max} \leq 6.0$; $H_{\max} =$

25 km for $M_{\max} = 7.0$; $H_{\max} = 30$ km for $M_{\max} = 7.5$; $H_{\max} = 40$ km for $M_{\max} = 8.0$; and $H_{\max} = 50$ km for $M_{\max} = 8.5$.

The dip angle α° of the lineament plane, measured clockwise from the horizontal plane, ranges from 0° to 180° , and the strike azimuth Az° ranges from 0° to 360° .

The lineaments and their segments may differ in their strike due to regional tectonic features and may intersect with each other, thereby enhancing the estimated seismic risk of their disjunctive nodes, because seismic effects produced by adjacent sources are summed. Predictive generation of the time–space and magnitude distributions of sources along lineaments (for example, calculation of ground motions, see Fig. 11) is usually subject to the conditions for “piercing” the ends of lineaments and their segments by large earthquake sources. In our calculations, the $M \geq 7.5$ sources of the size L_M are allowed to lie beyond the lineament limits over the distance $L/4$; for the $M \leq 7.0$ sources, this distance is $L/2$.

Real sources are scattered about the lineament axes by a value depending on the magnitude of associated earthquakes. We obtained the statistical mean values of these deviations for the entire territory of northern Eurasia (Table 2).

The rows in Table 2 list the standard deviations σ_M (km) of the $6.0 \leq M \leq 8.5$ earthquake sources from the principal lineament axes (M_{\max}) for a magnitude interval of $8.5 \leq M_{\max} \leq 6.0$ (the left column). One can see that, as M_{\max} decreases by a value n ranging from 0 to 2.5, σ_M increases and smaller sources are located at greater distances from the lineament axes, which

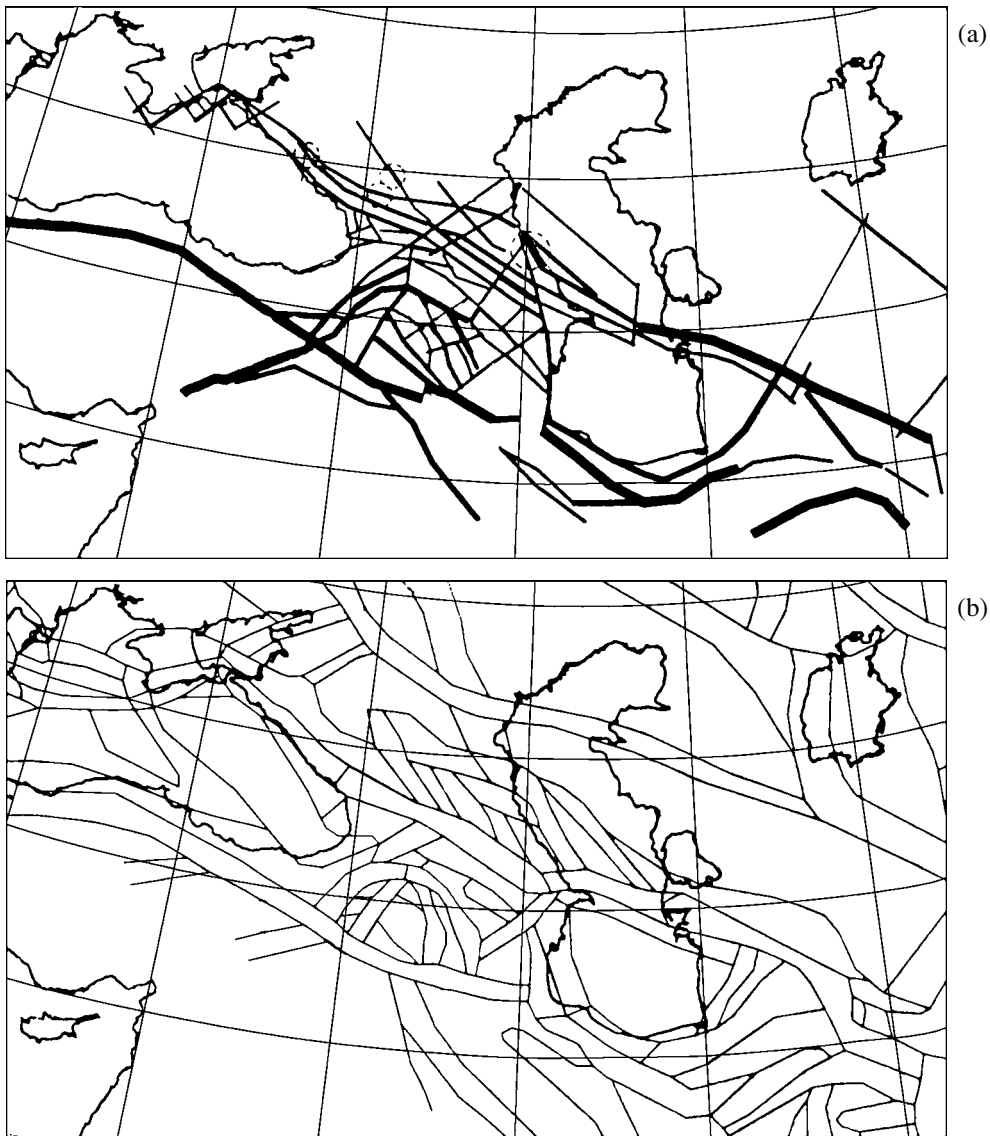


Fig. 7. A fragment of the LDS model of ESZs in the Crimea–Caucasus–Kopet Dagh region. (a) The lineament component of the LDF model. The solid lines, decreasing in thickness by a factor of 2, are lineaments with $M_{\max} = 8.0 \pm 0.2$; 7.5 ± 0.2 ; 7.0 ± 0.2 ; 6.5 ± 0.2 , and 6.0 ± 0.2 . Compiled by V. Ulomov and V. Trifonov (Russia), S. Nazaretyan and A. Avanesyan (Armenia), O. Varazashvili (Georgia), Khaled Hessami and Farshad Jamal (Iran), T. Ashirov and Ch. Muradov (Turkmenistan), and B. Pustovitenko and L. Borisenko (Ukraine). (b) The domain component of the LDF model. Thin lines are the conventional boundaries of the domains contrasting in their seismic regime [24]. The focal component of the LDS model is represented by potential earthquake sources with $M = 7.0$ (three sources) and $M = 7.5$ (one source). The sources, bounded by dashed lines in Fig. 7a, are shown only for the Russian territory of the northern Caucasus (after the data obtained by the recognition image method [25] and by the epicentral distance method [13–15]). Key: 1. b

resembles our fractal lattice model (Fig. 3). The values of $3\sigma_M$ (km) actually define the limiting width of the scatter band for all sources of earthquakes with $6 \leq M \leq M_{\max}$ and correspond to the size of the area, dynamically affected by the lineament structures with M_{\max} . These structures vary in size from $L_{M_{\max}}/2$ (where $L_{M_{\max}}$ is the source length) for large magnitudes and almost coincide with the source length for moderate M_{\max} . The values of σ_M given in Table 2 were further

used for trial localizations of the $M = M_{\max} - n$ earthquake sources relative to the associated lineament axes. For this purpose, seismic source data were randomly sampled from a special model catalog, which was numerically created for a long time interval (50 000 yr), taking account of a long-term average seismic regime (see Fig. 11). The scatter of the sources of earthquakes with smaller magnitudes at greater distances from lineament axes provided a relatively smooth transition from the determinate structure of source seismicity,

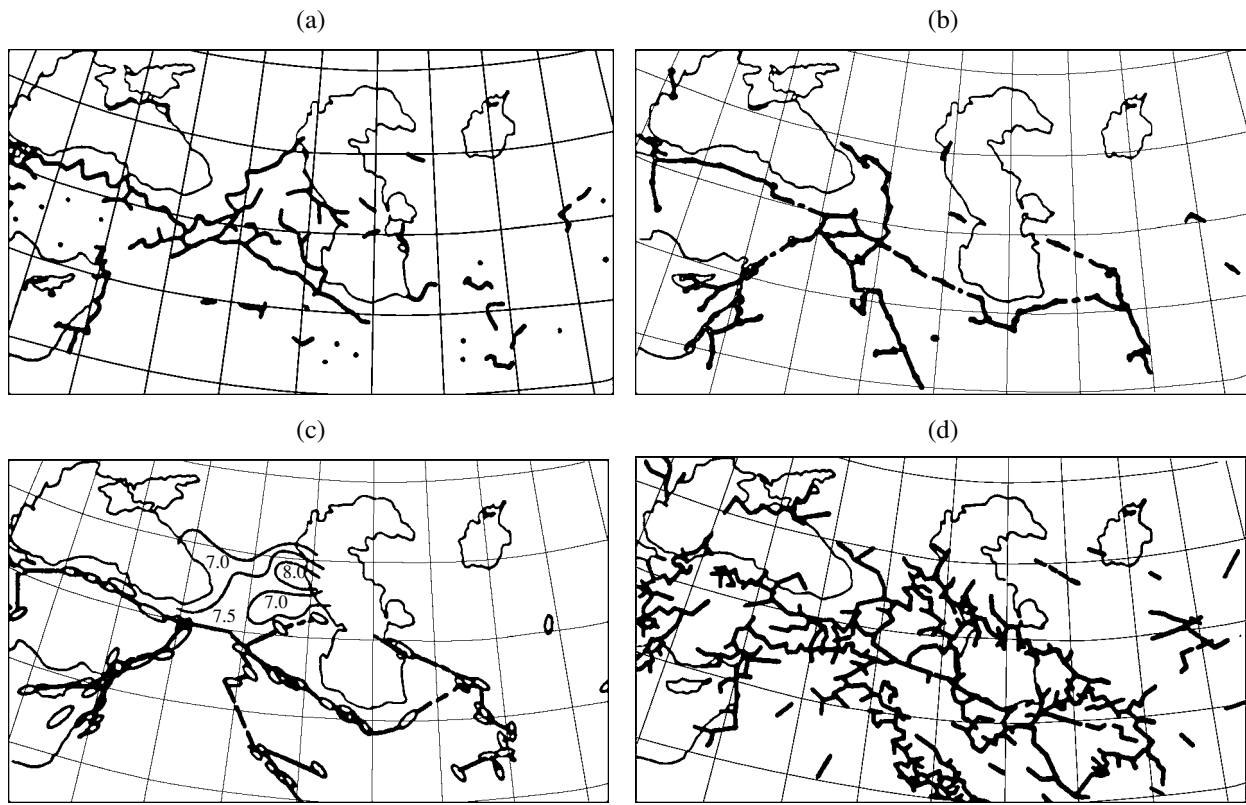


Fig. 8. Spatial clustering (without regard to the time factor) of seismic sources in the Crimea–Kopet Dagh region, based on the prevailing epicenter–epicenter distances (EED) of the earthquakes differentiated according to magnitude intervals of $\Delta M = M \pm 0.2$: (a) $M = 6.0$, (b) $M = 7.0$, (c) $M = 7.5$ and 8.0 . The contours of $M = 7.0$, 7.5 , and 8.0 , obtained by the EED method, show potential sources. (d) Clustering of the $M \geq 3.5$ earthquake hypocenters, with the sources in the lower crust ($h > 30$ km) and upper mantle (the boundaries separating the major blocks are clearly outlined).

represented by lineaments, to domains with their scattered sources of smaller earthquakes.

Domains (d) are less structurized areas or insufficiently studied seismogenic zones characterized by weak seismicity (in our case, $M \leq 5.5$) and quasi-homogeneous tectonics. Domains related to lineaments and caused by their dynamic influence are the first-order domains (d_l), whereas domains located separately from lineaments and delineated from seismic and seismogeological evidence are referred to as the second-order domains (d_d). They reflect the background component of local seismicity and seismotectonics. The former complement, without gaps, the seismic regime around lineaments by weak earthquakes ($M \leq 5.5$),

whereas the latter are considered independently and may have any value of M_{\max} characteristic of the domain.

Unlike seismic lineaments, the domains do not intersect and cover the entire territory, without gaps and superpositions (an apparent intersection may be inherent in the domains belonging to different deep layers, for example, on the Kuriles, in the Hindu Kush, Carpathians, and other regions). For convenience of further calculations, the domains contours (like lineaments) are consecutively discretized to obtain broken lines, without gaps and in the same direction (for example, clockwise). As noted above, the introduction of domain models (as well as the concept of “quasi-homogeneous

Table 2

M_{\max}	$\sigma_M, M_{\max} - 0$	-0.5	-1.0	-1.5	-2.0	-2.5	$3\sigma_m = 6.0$	$L_{M_{\max}}$
8.5	12	17	25	35	51	73	219	400
8.0	10	15	21	30	43		129	200
7.5	9	12	18	25			75	100
7.0	7	10	15				45	50
6.5	6	9					27	25
6.0	5						15	13

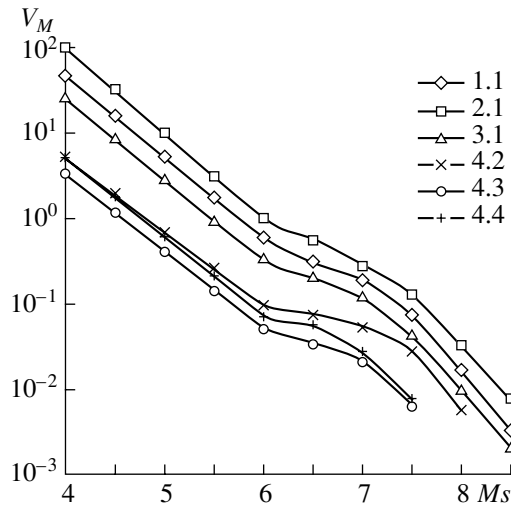


Fig. 9. Yearly average flux rate V_{LH} of the $M \geq 4.0$ seismic events in the main North Eurasian regions, with an allowance made for an excess in the observed seismic activity V_0 of earthquakes with $M \geq 6.5$ over the activity V_c calculated from the exponential law characteristic of the recurrence of events with $4 < M \leq 6.0$. This law yields the following regional equations: 1.1. $\log V_M = 1.676 - 0.970(M - 4)$ for the Iran–Caucasus–Anatolia region (GSHAP test area, $S = 1800000 \text{ km}^2$); 2.1. $\log V_M = 2.002 - 1.011(M - 4)$ for Central Asia ($S = 2300000 \text{ km}^2$); 3.1. $\log V_M = 1.423 - 0.970(M - 4)$ for the Altai–Sayany–Baikal region ($S = 2700000 \text{ km}^2$); 4.2. $\log V_M = 0.686 - 0.863(M - 4)$ for the Sakhalin–Japan region ($S = 900000 \text{ km}^2$); 4.3. $\log V_M = 0.526 - 0.913(M - 4)$ for the Amur–Primorski Krai region ($S = 500000 \text{ km}^2$); 4.4. $\log V_M = 0.742 - 0.951(M - 4)$ for the Verkhoyansk region. The exponential V_M equations ($M = 4–6$) describes the areas S in which the epicenter concentration is no less than three per ten thousand of square kilometers.

seismotectonic provinces") is caused by the impossibility to reveal a finer seismicity structure from weak earthquakes, due to large errors in localizing their epicenters, which exceed the typical distances between the epicenters and thereby the step of tectonic lattice of the same hierarchy. However, in reality, the seismicity is structurized at all scale levels, and more careful studies can lower the magnitude level of lineaments. Such an approach is also applicable to studying the fractal processes in the sources themselves, foreshock and aftershock sequences, and other grouped events of various hierarchical levels [23].

The focuses of potential sources (f_i) identified by various methods (from coseismic ruptures, prevailing inter-epicenter distances, recognition of images, etc.) are commonly restricted to seismic lineaments, and in view of (2), the source size L_{JM} is related to the maximum potential earthquake magnitude.

In the VLSI technology, all of the three basic structural ESZ elements (seismic lineaments, domains, and potential sources), as well as the whole remaining database, are represented as individual electronic layers. At the final stage of the seismic risk assessment (see Fig. 1), the seismic effect I_i on the Earth's surface is independently

evaluated for each structural element, and the relevant information is stored at the nodes of the square grid covering the entire territory examined. As a result, this allows us to map the contours of ground motion intensity I_i , with a given probability and in given time intervals.

Magnitude Parametrization of Source Zones

Like earthquakes, the ESZs are classified according to the following gradation of magnitudes M_{LH} : $M \leq 8.0 \pm 0.2$; $\leq 7.5 \pm 0.2$; $\leq 7.0 \pm 0.2$; $\leq 6.5 \pm 0.2$; $\leq 6.0 \pm 0.2$; $\leq 5.5 \pm 0.2$; $\leq 5.0 \pm 0.2$; $\leq 4.5 \pm 0.2$; $\leq 4.0 \pm 0.2$; and $\leq 3.5 \pm 0.2$. The upper threshold (M_{\max}) is determined by a real seismotectonic and seismogeodynamic situation, and the lower threshold (M_{\min}) depends on the recording reliability (completeness) of minimum magnitude earthquakes that are still seismically hazardous (in our studies, we assumed $M_{\min} = 4.0$ and $I_{\min} = 5$). M_{\max} is estimated by all of the available and reasonable methods: from the paleoseismic rupture sizes, archaeological and historical monuments, width of dynamic influence zones of main seismogenic structures, length and segmentation of seismically active faults and lineaments, sizes of interacting blocks, bend of earthquake recurrence curves, extrema in the accumulated strain curves for seismogenic structures, potential sources with the maximum magnitude revealed by various methods, etc.

In accordance with the fractal structure of a hierarchical geophysical medium described by the lattice model, the sources of the largest earthquakes with $M = M_{\max}$, $M = M_{\max} - 0.5$, and $M = M_{\max} - 1$ are located more or less regularly along the lineaments $l_{M_{\max}}$ (see the principal lineaments in Fig. 3b). The sources of smaller earthquakes with $M = M_{\max} - 1.5$, caused by the dynamic influence of large lineaments, are scattered in the domains d_l adjacent to the seismic lineaments. Such a concentration and higher recurrence of large earthquakes on lineaments (faults) are consistent with the concepts of "characteristic" earthquakes [10, 26–28], as is also confirmed by our nonlinear plots of seismic activity in continental regions of northern Eurasia [15, 23]. Figure 9 shows that the exponential recurrence law is violated for seismic events in the interval $M \geq 6.5$. This reflects a higher frequency of moderate and large earthquakes compared to that derived from the logarithmic linear extrapolation of data on weak earthquakes. To a first approximation, such a phenomenon can be explained by layering of the crust and upper mantle: large sources extend beyond an upper (e.g. granitic) layer and penetrate the lower layers having a different strength and dynamic properties. However, the nonlinearity is somewhat removed by using, instead of M_{LH} , a physically more adequate moment magnitude M_w [28, 29] in the magnitude classification. In any case, this effect must be taken into consideration in the seismological parametrization of earthquake sources and in the assessment of their seismic risk, since the real fre-

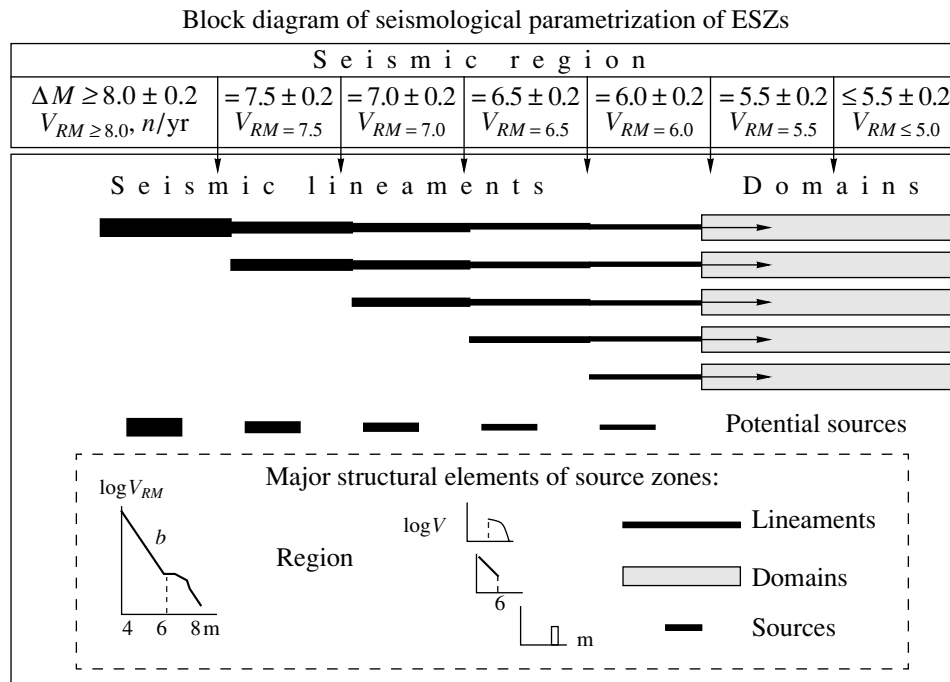


Fig. 10. Block diagram of the seismological parametrization of ESZs.

quency of the earthquake occurrence, for example with $M \geq 7.0$, is three and more times higher than that expected from the exponential approximation of all values of V_M in a wide magnitude interval ($4.0 \leq M \leq 8.5$). This can be seen most clearly in the data processing by the maximum likelihood method (Fig. 9).

Since any natural seismicity has a certain structure, the lower limit of M_{\max} in lineaments can be arbitrary, depending on the accuracy of seismological and seismotectonic reconstructions. For the general seismic zoning (GSZ) on a scale of 1: 2 500 000 and smaller, this value is usually not lower than $M_{\max} = 6.0$, and in the detailed assessment of seismic risk of especially important objects, the lower magnitude threshold can be lowered.

The d_d domains are characterized by a relatively low magnitude M_{\max} , since they are commonly located in poorly structurized, low-seismicity plain territories or fill the space between the widely spaced lineaments of large and moderate magnitudes, reflecting the background seismicity (see Fig. 5, on the left).

Potential sources f_i and associated lineaments are commonly characterized by M_{\max} , strike azimuth Az° , length L_{JM} , depth to their geometric center (H_c) or upper edge (H_{\min}), source motion type, and, if possible, recurrence period (for example, determined from coseismic paleorupture datings). In highly active regions, potential sources with large magnitudes ($M \geq 7.0 \pm 0.2$) are important, whereas in weakly active regions, potential sources of smaller earthquakes may be significant.

Seismic Regime of Source Zones

In the probabilistic seismic zoning, the reliability of the seismic risk assessment in a particular area depends not only on M_{\max} , but to an equal degree on the determination reliability of space-time and energy parameters of the seismic regime. For this reason, the method for seismic parametrization described below is important. It is convenient to consider this method separately for structural ESZ elements of different types (naturally, bearing in mind their interrelation).

Seismic lineaments. The recurrence of earthquakes of various magnitudes on seismic lineaments is determined as follows.

For each genetically coherent seismic region (usually 2000 to 3000 km in length and 500 to 1000 km in width [14, 15]) and for each magnitude interval $\Delta M = \pm 0.2$, an average flux rate V_{RM} of these events is determined, based on the earthquake catalog free of aftershocks, foreshocks, and other collective events. This flux rate is the number N_{RM} of earthquakes with the specified magnitudes per one year or the yearly-average probability $P_{RM(1)}$ of the occurrence of at least one of such earthquakes in region R , with allowance made for the representativeness of seismic events sampled. As noted above, we assumed that ESZ events with $M \geq 6.0$ belong to lineaments and potential sources, and ESZ earthquakes with $M \leq 5.5$ belong to the related domains (see Figs. 9–11).

Further, assuming that each magnitude M of seismic lineaments has its own regional earthquake recurrence plot (Fig. 9), the values of V_{RM} for $M \leq 6.0$ are distrib-

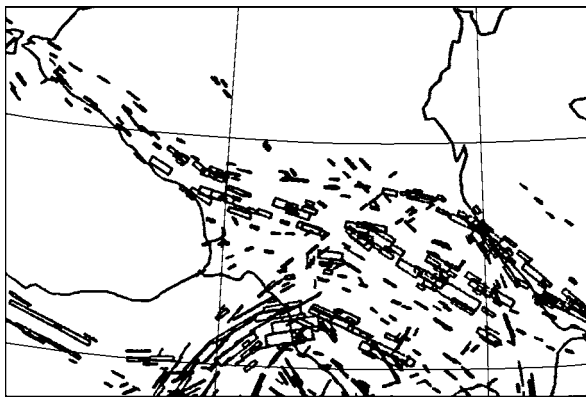


Fig. 11. A fragment of the long-term seismicity prediction map for the Caucasus and adjacent Turkish territory for the nearest 500-yr interval. Synthesized sources are shown as the projections of the horizontally extended rectangles (in principle, these may be ellipses) onto the Earth's surface; the rectangle size is related to the magnitude of possible earthquakes (in the given case, $M \geq 6.0$). The width of the rectangles depends on the fault plane dip angle. The map was constructed with the help of the software package developed by A.A. Gusev and V.M. Pavlov, with the participation of L.S. Shumilina and V.I. Ulomov.

uted over V_{li} , between the corresponding seismic lineaments proportionally to their length l_i (with the weighting coefficients W_{li}):

$$V_{li} = V_{RM} W_{li}, \quad (6)$$

where V_{RM} is the flux rate of events with a specific M in the region, V_{li} is the flux rate of the same events in each of the seismic lineaments l_i with $M_{\max} = M$ and in all of the higher-rank lineaments, since the latter also include the events with the magnitude considered (Fig. 10).

The value of W_{li} is calculated from (7), assuming that (in accordance with the lattice model in Fig. 3b) the seismic activity of the lineaments of a fixed rank is constant within the entire region (as stated below, this can be achieved, if necessary, by dividing the region into more homogeneous subregions):

$$W_{li} = l_i / \Sigma l_i, \quad (7)$$

where l_i is the length of the i th lineament in which earthquakes of magnitude M are possible, and Σl_i is their total length characterizing the total flux rate V_{RM} of seismic events with the given M in the region. Furthermore, according to the aforesaid, all lengths of the higher-rank lineaments (if they exist) whose magnitudes exceed M_{\max} are also summarized (Fig. 10). Thus, in the magnitude interval $\Delta M = 6.0-8.5$, the summary length of lineaments with $M = 7.5$ also includes lengths of all lineaments with $M \geq 8.0$; for $M = 7.0$, this length includes the summary length of lineaments with $M = 7.5$ and $M \geq 8.0$; etc.

The procedure described above can be repeatedly applied to subregions highly contrasting in their seismic activity (for example, the eastern and western parts

of the Greater Caucasus (Fig. 6). Note that the transverse size of a subregion must be no less than $\delta_M = 10^{0.6M - 1.94}$ (the diameter of the zone responsible for the earthquake with M_{\max}). The region can be easily divided into subregions by representing all the lineaments as individual segments with their own geometric and seismic parameters. However, such a division is not always justified, since different concentrations of lineaments in various parts of the region are already evidence of the differentiation in its activity, and a practical test of this version confirmed it.

At the final stage, the histogram of the distribution of the earthquake recurrence period T_{li} over all magnitude intervals under consideration is constructed for each lineament, using (6):

$$T_{li} = 1/V_{li}. \quad (8)$$

To estimate the seismic risk and compare the seismic activity of lineaments in various regions and subregions, as well as for other applications, V_{li} and T_{li} are normalized not only in time, but also in distance (along the lineaments), to a length of 100 km. Then, (6) and (8) take the form

$$V_{li}^* = (V_{li} 10^2) / l_i; \quad T_{li}^* = l_i / (V_{li} 10^2). \quad (9)$$

Domains. The domains are parametrized by a simpler, ordinary method. As mentioned above, the magnitude of the maximum possible earthquakes in the domains usually does not exceed $M = 5.5$. The earthquake recurrence plots can also be easily constructed on the basis of a sample from a regional catalog for the area S_i of each domain and actually observed seismic activity level ($V_4 = \text{var}$, $b = \text{var}$), taking into account the recording representativeness of the events in question. This segment of the plots ($M = 4-6$) is almost always logarithmically linear, unlike the segment including events of greater magnitudes (see Fig. 9).

The yearly average flux rate V_{di}^* and recurrence periods T_{di}^* of events with various M are normalized to an area of 10^4 km^2 :

$$V_{di}^* = (V_{di} 10^4) / S_i; \quad T_{di}^* = S_i / (V_{di} 10^4). \quad (10)$$

Obviously, the absolute estimates of the seismic regime can be obtained for each of these main structural ESZ elements through multiplying or dividing (9) by the length of the relevant seismic lineaments. The same can be obtained by multiplying or dividing (10) by the area of the relevant domains.

We see that, in the case of the parametrization of the domain components of the LDS model, no weighting coefficients are required, since the whole long-term set of seismic events in each of the domains already characterizes its seismic regime in both space and time. However, when constructing the recurrence curve, one should not forget that the transverse size of the domains must not be smaller than $\delta_M = 10^{0.6M - 1.94}$ (the size of the

zone responsible for the greatest magnitude M in the domain).

Potential sources

Potential sources of earthquakes (f_i), as already noted, represent the third type of the structural ESZ elements and an individual electronic layer in the data bank of the VLSI technology. They are more or less reliably recognizable by various methods [e.g., 22, 25] and can play an important role in the seismological parametrization of source zones and in the seismic risk assessment. In highly active regions, the potential sources with $M \geq 7.0 \pm 0.2$ are most significant. In low-activity regions, the lower magnitude level may be diminished.

The majority of potential sources of large magnitudes are related to seismic lineaments, and those of smaller magnitudes can belong to domains. This determines the method of their seismogeological parametrization. The former have the length $l_{fi} = L_{fi}$ and represent the most dangerous segments of the related lineaments. They are considered as independent short seismic lineaments, being included in the general parametrization procedure. However, since only the earthquakes with fixed M_{\max} are expected in the potential sources, the length l_{fi} of potential risk zones is taken into consideration only when the flux of events V_{RM} is distributed among the lineaments of the same rank (M_{\max}). In the flux distribution of events of all other magnitudes, the length l_{fi} is neglected.

The M_{\max} value of potential sources can either exceed (see Figs. 5, 7) or coincide with M_{\max} of the related lineament. However, in the latter case, the role of potential sources also remains substantial, since the flux of seismic events with M_{\max} and, consequently, the seismic risk in these parts increase, at least, two times due to both the activity of the source itself and the activity of the lineament segment covered by the source. According to our studies of the distribution function $P(\delta_M)$ of prevailing epicenter–epicenter distances δ_M for earthquake sources with $6.0 \leq M \leq 8.0$ in the continental North Eurasia, the probability that the potential source of the size L_{fM} would lie on a segment of the length $l_{fM} = 2L_{fM}$ is approximately $P_{(L/M)} = 0.7$ on each of the lineament segments of the length δ_M .

Performing numerical experiments with a model earthquake catalog in accordance with a certain scenario designed in terms of the FLM, we can approach a more realistic distribution of earthquake sources, including the potential sources. For example, this can be achieved by specifying a distribution function of the source probability density at “prevailing” epicenter–epicenter distances and by precluding the repeated source occurrence at the same place before the accomplishment of the recurrence cycle in the entire lineament.

Figure 11 shows a fragment of the long-term (500 years) seismicity prediction map in the form of synthetic sources of earthquakes with $M \geq 6.0$ in the Caucasus and northeastern Turkey. For simplicity, the map of Fig. 11 was constructed only on the basis of the lineament component of the ESZ model (i.e., neglecting the domains and potential sources, see Fig. 7a), by means of a random sample from a long-term (50000 years) model catalog. In practice, when evaluating the seismic risk, the 500-yr period corresponds to the probability that seismic effects in the region would not exceed 90% of their maximum in the nearest 50 yr; however, mean values of a great number of samples are considered here.

The seismic sources are shown in Fig. 11 as the projection onto the horizontal plane of rectangles whose size is proportional to the magnitude of predicted earthquakes. In the same random manner, using the data of Table 2, a scatter of sources was generated about the axes of corresponding lineaments, and their spatial orientations were obtained from strike azimuths and dip angles (in the given case, two intervals of dip angles of $90^\circ \pm 20^\circ$ and $45^\circ \pm 20^\circ$ were chosen experimentally).

Considering the migration processes along lineaments and the history of seismic events at a potential source, we can change the estimated probability of the forthcoming earthquake occurrence, for example, by superimposing a few segments l_{fi} (or by making a proper gap at a given place of the main lineament).

Assuming that the Poisson distribution of the annual average flux V_{fM} of seismic events is stationary (at least, over some interval of time) and knowing the date t_1 (year) of the last seismic event with M_{\max} at the source under consideration, we can estimate the probability $P_1(t)$ that the next earthquake would occur here during a time interval $\Delta t = t_2 - t_1$ (i.e., before the t_2 year) using the formula

$$P_1(t) = 1 - e^{-V_{fM}\Delta t}. \quad (11)$$

If the potential sources with $M = M_{\max}$ are located within domains d_d isolated from lineaments, the recurrence period T_{fi} of the events with M_{\max} can be calculated from an individual earthquake recurrence plot:

$$T_{pi}(M) = 10^{b(M-4)} / 10^{V_4}, \quad (12)$$

based on a sample from the regional catalog of seismic events within a circle of radius $\rho_{M_{\max}} = \delta_M/2$,

$$\rho_{M_{\max}} = 10^{0.6M-2.19}. \quad (13)$$

If the number of seismic events in this circle is insufficient for the calculation of their flux rate, the $M = M_{\max}$ earthquake recurrence period can be calculated from geological data, specifically, from the average rate V_g (cm/yr) of recent differentiated tectonic movements in the vicinity of potential sources, using the formula

$$T_g(M) = (10^{0.6M-2.0}) / V_g. \quad (14)$$

Geological data are also important for all other aspects of the numerical ESZ parametrization: identification and classification of blocks and lineaments, delineation of tectonically quasi-homogeneous zones (domains), estimation of the minimum depth to the upper boundary of an earthquake source and the thickness of a seismically active layer, and other seismogeodynamic reconstructions.

CONCLUSION

Earthquakes occur in a discrete block-layered medium, the structure and dynamics of which are determined by the previous geological epochs and, in the long run, are caused by the Neogene–Quaternary and present tectonic movements. The relation between large active geostructures and seismicity is clearly expressed not only on a global scale, as regular zones of recent and ancient subduction and rifting, but also at a regional level, as the fractal hierarchy of lineaments and blocks reflecting the fault tectonics and fractal distribution of earthquake sources. These and many other regularities indicating the structural–dynamic coherence of the geological medium and seismogeodynamic processes allowed us to create geometrically ordered, physically reasonable fractal lattice model of seismogeodynamics, which is capable of providing a deeper insight into seismogenesis.

Identifying seismogenic structures with lineaments, we continue the progressive traditions of the Russian school of seismogeologists, founded by I.V. Mushketov and A.P. Orlov [31, 32] at the end of the past century and developed by I.E. Gubin [1] and other domestic scientists in the middle of this century. The representation of seismogenic structures as “quasi-homogeneous seismotectonic provinces” (domains in our terminology) with their scattered seismicity, which has been widely accepted until recently, is less realistic from both the seismological and geotectonic standpoints. However, although the scattered seismicity does not actually exist in nature, we have to use such an approach, as well as the domain model, because our knowledge of the fine structure of the seismic medium is incomplete. In this respect, the most rational way is to construct a hybrid lineament–domain ESZ model which was developed in this paper. However, the overall replacement of high-amplitude lineaments by areal domains is unacceptable for physical reasons. Moreover, this is unjustified for the following two reasons. First, a decrease in the domain area without regard to the size of zones responsible for large earthquakes increases the recurrence period of such events and, consequently, underestimates the seismic risk, resulting in errors of the “missing target” type in seismic zoning maps. Second, an excessive enlargement of the domains within which high-magnitude earthquakes are possible makes the seismic risk pattern more diffuse and gives rise to errors of the false alarm type.

The lineament–domain–focal ESZ model, based on the probabilistic–determinate fractal lattice regularization of the parameters of regional seismicity and recent geodynamics avoids these shortcomings and adequately incorporates the specific features of the distribution of earthquake sources for various magnitudes [35]. Another innovation is the practical use of extended, rather than concentrated, seismic sources, adequate to the real natural conditions, in the seismic risk assessment and mapping.

The new method of creation of the ESZ models and their application to the seismic zoning was named “Earthquake Adequate Source Technology – EAST-97”.

ACKNOWLEDGMENTS

I am deeply grateful to L.S. Shumilina and N.S. Medvedeva for useful discussions and their help in many numerical experiments.

REFERENCES

1. Gubin, I.E., *Seismotektonicheskii metod seismicheskogo raionirovaniya* (Seismotectonic Method of Seismic Zoning), Trudy Geofiz. instituta AN SSSR (Proc. Geophys. Inst. Acad. Sci. SSSR), 1950, no. 13(140).
2. Medvedev, S.V., *Voprosy seismicheskogo raionirovaniya* (Problems of Seismic Zoning), *Byull. Soveta po seismologii* (Bulletin of Seismological Council), 1960, no. 8.
3. Riznichenko, Yu.V., From the Earthquake Source Activity to Ground Motions, *Izv. Akad. Nauk SSSR, Fiz. Zemli*, 1965, no. 11, pp. 1–12.
4. Kantorovich, L.V., Keilis-Borok, V.I., and Molchan, G.M., (1974), Seismic Risk and Principles of Seismic Zoning. Series: Seismic Design Decision Analysis, *Internal Study Report*, Department of Civil Engineering, MIT, no. 43.
5. Cornell, C.A., Engineering Seismic Risk Analysis, *Bull. Seismol. Soc. Am.*, 1968, vol. 58, pp. 1583–1906.
6. Algermissen, S.T. and Perkins, D.M., (1976). A Probabilistic Estimation of Maximum Acceleration in the Contiguous United States, *USGS Open-File Report 76-416*.
7. McGuire, R.K., FORTRAN Computer Program for Seismic Risk Analysis, *USGS Open-File Rep. 76-77*, 1976, p. 90.
8. Bender, B. and Perkins, D.M., SEISRISK III: a Computer Program for Seismic Hazard Estimation, *U. S. Geol. Surv. Bull.*, 1987, vol. 1772.
9. Gao, M., The Joint Probabilistic Model of Space and Magnitude and Its Application to Seismic Zonation, *Proc. Joint Conference of Asia on Earthquake, Osaka, Japan, October 29–November 2*, 1993.
10. Wu Shen-Chyun, Cornell, C.A., and Winterstein, S.R., A Hybrid Recurrence Model and Its Implication on Seismic Hazard Results *Bull. Seismol. Soc. Am.*, 1995, vol. 85, no. 1, pp. 1–16.
11. *Seismicheskoe raionirovanie territorii SSSR. Metodicheskie osnovy i regional'noe opisanie karty 1978 goda* (Seismic Zoning of the USSR Territory: Underlying

- Methods and Regional Legend of the Map of 1978), Moscow: Nauka, 1980.
12. Global Seismic Hazard Assessment Program, *Ann. Geofiz., Spec. Issue: Technical Planning Volume of the ILP'S*, 1993, vol. XXXVI, no. 3-4.
 13. Ulomov, V.I., A Lattice Model of the Focal Seismicity and Seismic Danger Prediction, *Uzb. Geol. Zh.*, 1987, no. 6, pp. 20–25.
 14. Ulomov, V.I., Regional Seismicity Structures and Some Aspects of Seismic Zoning in Eurasia, *Proceedings of PRC, USSR Workshop on Geodynamics and Seismic Risk Assessment, Beijing, China, 1991*, Seismol. Press, 1993, pp. 283–301.
 15. Ulomov, V.I., Global Ordering of Seismogeodynamic Structures: Implications for Seismic Zoning and Long-Term Earthquake Prediction, *Seismichnost' i seismicheskoe raionirovanie Severnoi Evrazii* (Seismicity and Seismic Zoning of North Eurasia), vol. 1, Moscow: OIFZ RAN, 1993, pp. 24–44.
 16. Ulomov, V.I., Structural and Dynamical Regularity of Eurasia Seismicity and Some Aspects of Seismic Hazard Prediction, *European Seismological Commission, XXIV General Assembly, 1994, September 19–24, Athens, Greece, Proceedings and Activity Report, 1992–1994*, vol. 1, pp. 271–281.
 17. Ulomov, V.I., International Workshop “Methods and Algorithms in Studies of Regional Seismicity and Seismic Risk Analysis in the Crimea–Caucasus–Kopet Dagh Region”, *Fiz. Zemli*, 1995, no. 5, pp. 92–96.
 18. Kostrov, B.V. and Shamita Das, *Principles of Earthquake Source Mechanics*, Cambridge: Univ. Press, 1988.
 19. Kasahara, K., *Mekhanika zemletryasenii* (TRANSI), Moscow: Mir, 1985.
 20. Grigoryan, S.S., Focal Mechanisms of Earthquakes and Empirical Seismological Relationships, *Dokl. Akad. Nauk SSSR*, 1988, vol. 299, no. 5, pp. 1094–1101.
 21. Sobolev, G.A., *Fizika ochaga i prognoz zemletryasenii* (Source Physics and Prediction of Earthquakes), Moscow: Geofiz. Tsentr RAN, IFZ RAN, 1992.
 22. Ulomov, V.I., Seismogeodynamic Activation Waves and Long-Term Earthquake Prediction, *Fiz. Zemli*, 1993, no. 4, pp. 43–53.
 23. Ulomov, V.I., *Dinamika zemnoi kory Srednei Azii i prognoz zemletryasenii* (Crustal Dynamics of Central Asia and Earthquake Prediction), Tashkent: FAN, 1974.
 24. Shebalin, N.V., Ulomov, V.I., Tatevossian, R.E., Trifonov, V.G., Ioffe, A.I., and Kozhurin, A.I., Unified Seismogeological Taxonomy of the Northern Eurasia, *IUGG-Abstracts, SB21C-14*, Boulder, 1995.
 25. Reisner, G.I. and Ioganson, L.I., Seismic Potential of Western Russia and Other CIS and Baltic Countries, *Seismichnost' i seismicheskoe raionirovanie Severnoi Evrazii* (Seismicity and Seismic Zoning of North Eurasia), Moscow: OIFZ RAN, 1993, pp. 186–195.
 26. Youngs, R.R. and Coppersmith, K.J., Implications of Fault Slip Rates and Earthquake Recurrence Models for Probabilistic Seismic Hazard Estimates, *Bull. Seismol. Soc. Am.*, 1985, vol. 75, pp. 939–964.
 27. Wesnousky, S.G., Earthquakes, Quaternary Faults, and Seismic Hazard in California, *J. Geophys. Res.*, 1986, vol. 91, pp. 12587–12631.
 28. Wu Shen-Chyun, Cornell, C.A., and Winterstein, S.R., A Hybrid Recurrence Model and Its Implication on Seismic Hazard Results, *Bull. Seismol. Soc. Am.*, 1995, vol. 85, no. 1, pp. 1–16.
 29. Hanks, T.C. and Kanamori, H., A Moment Magnitude Scale, *J. Geophys. Res.*, 1979, vol. 84, pp. 2348–2350.
 30. Gusev, A.A. and Mel'nikova, V.N., World-Average and Kamchatka Magnitude Relations, *Vulkanol. Seismol.*, 1990, no. 6, pp. 55–63.
 31. Orlov, A.P., *O zemletryaseniyakh voobshche i o zemletryaseniyakh Yuzhnoi Sibiri i Turkestanskoi oblasti v osobennosti* (General Remarks on Earthquakes, with Special Reference to South Siberia and Turkestan), *Trudy Obshchestva estestvoispytatelei pri Kazanskom universitete* (Proc. Kazan University Society of Natural Sciences), 1872, vol. 3, no. 1, issue 1.
 32. Mushketov, I.V., Materials Concerning the Study of Earthquakes in Russia, *Izv. Russ. Geogr. Ob-va*, 1891, issue 1; 1899, issue 2.
 33. Ulomov, V.I., Main Aspects and Technical Suggestions with Regard to the Construction of the Seismic Zoning Map on the Territory of the Russian Federation, *Seismichnost' i seismicheskoe raionirovanie Severnoi Evrazii* (Seismicity and Seismic Zoning of North Eurasia), vols. 2–3, Moscow: OIFZ RAN, 1995, pp. 9–26.
 34. Ulomov, V.I., Regional Seismicity Structures, *Sovremen-naya dinamika litosfery kontinentov. Povizhnye poyasy* (Recent Dynamics of the Continental Lithosphere: Mobile Belts), Logachev, N.A. and Khromovskikh, V.S., Eds., Moscow: Nedra, 1995, pp. 401–419.
 35. Ulomov, V.I., On the Identification and Seismological Parameterization of Earthquake Source Zones. The Caucasus and Adjacent Area, *Historical and Prehistorical Earthquakes in the Caucasus, NATO ASI, Series 2: Environment*, vol. 28, ILP Publication no. 333, Dordrecht: Kluwer Academic, 1997, pp. 503–522.